INSTITUTE FOR NUCLEAR STUDY
UNIVERSITY OF TOKYO
Tanashi, Tokyo 188
Japan

INS-TH-160
June 23. 1984

# Test of the Wire Pattern of the TOPAZ Inner Drift Chamber

K. Kono, A. Imanishi, T. Ishii, S. Kato, H. Masuda, T. Morimoto,
K. Norimura, T.Ohshima, H.Okuno, K. Shiino, K. Ukai and M. Yoshioka

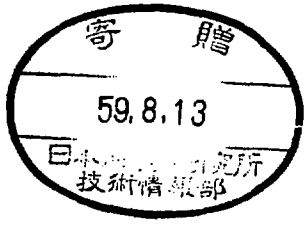

INS-TH-160

# Test of the Wire Pattern of the TOPAZ Inner Drift Chamber

K. Kono, A. Imanishi, T. Ishii, S. Kato, H. Masuda,
T. Morimoto, K. Norimura, T. Ohshima, H. Okuno, K. Shiino,
K. Ukai and M. Yoshioka

Institute for Nuclear Study, University of Tokyo

( June 23, 1984 )

We have tested two wire patterns for the TOPAZ inner drift chamber. In the magnetic field of 6kG, the hexagonal drift cell gives the better x-t relation than the square drift cell. The mean spatial resolution of 110 $\mu$m is obtained with the gas mixture of Ar(50%)/$C_2H_6$(50%).

## 1. Introduction

A TOPAZ inner drift chamber (IDC)[1] is designed (1) as a fast triggering element for charged particles and (2) as a tracking element closest to the beam crossing area. The sensitive area of the IDC is shown in Fig.1. The inner diameter and the outer diameter of the IDC are 200mm and 590mm, respectively. Its length in the beam direction is 1510mm. The end-plate of the IDC is schematically shown in Fig.2. Ten layers of anode wires are placed co-cylindrically, where neighbouring two layers are staggered to solve the left-right ambiguity. Inner four layers have 64 anode wires each and outer six layers have 128 anode wires each. As shown in Fig.2, each pair of layers are separated with the cathode cylinder made of paper-honeycomb structures. The z-information in the IDC is obtained from the zig-zag delay line placed on both surfaces of the honeycomb cylinder.

As we intend to extract both the drift time information and the cathode-induced signal information with good accuracy, the wire configuration should be carefully studied. Also the IDC will be used under the magnetic field of 10kG, the geometry of the wire configuration would have much effect on the space-time relation and on the spatial resolution of the drift chamber.

We have studied two possible patterns of the wire configuration under the magnetic field of 6kG.

## 2. Test Chamber

The drift chamber used in the present test is shown in Fig.3. The chamber box has a dimension of 120mm x 195mm x 150mm.

Fifty anode wires (gold-plated tungusten wire of 30 $\mu$m in diameter) and 110 potential wires (copper-beryllium wire of 100$\mu$m in diameter) were placed as shown in the figures. For the accurate positioning of the anode wires, ruby balls with the hole of 50$\mu$m in diameter is used.

Two wire patterns, No.1 and No.2, are tested. The No.1 pattern has a rectangular drift cell of 5 mm x 6 mm. In the No.2 pattern, the wire cathode plane is shifted by a half cell so that the unit drift cell has a hexagonal shape.

The calcurated equi-drift-time maps for each wire configration are shown in Fig.4, where results without and with the magnetic field of 6kG are shown for both wire patterns. In this calculation, the data by K. Fujii et al[3] was used for the electron drift velocity in the gas mixture of Ar(50%)/$C_2H_6$(50%).

## 3. Test Setup

Experimental setup is shown in Fig.5. The momentum-analyzed electron beam (500MeV/c) was produced by the bremsstrahlung photon beam from the 1.3 GeV electron synchrotron. The test chamber was placed in the magnetic field of the large aperture magnet (LAM) whose effective field volume was 50cm x 80cm x 50cm (width x length x height). The maximum field strength was 6 kG. Two triggering scintillation counters defined the electron beam trajectory.

The preamplifiers and discriminaters used in the present test was LRS-HIL440. Digital output signals were sent to the LRS-4291B Drift Chamber Digitizer via 30m-long twisted-pair

cables. The on-line data aquisition was done with the use of LSI 11/23 through CAMAC system.

## 4. Operation Test

The gas mixture used in the present test was Ar(50%)/$C_2H_6$(50%). Figure 6 shows the collected charge distributions for $^{55}Fe$ X-rays and for minimum-ionizing electrons. The preamplifier used for this charge measurement is LRS-MVL 100 with the differentiation time constant of 50ns. For $^{55}Fe$ X-rays, the pulse height is proportional to the ionization charge up to the H.V. region of 2.2kV. Above 2.5kV, the limited-streamer mode starts. For minimum-ionizing particles, the collected charge is about 36% of the $^{55}Fe$ 6keV peak, which corresponds to the energy loss of 2.1 keV. In the magnetic field of 6kG, no appreciable change was observed in the signal shape and in the signal amplitude.

Figure 7 shows the efficiency curves obtained with and without the magnetic field. The efficiency was measured for each laryer of anode wires. We define the anode layer number as shown in Fig. 3. As seen in Fig. 3, anode wires in the layer #2 and #3 are surrounded by potential wires only. On the otherhand, anode wires in the other layers face to the cathode plane on one side. Therefore electric-field strength near the anode wire differs slightly between both cases. This situation is apparently shown in Fig.7, where two efficiency curves are corresponding to two different anode layers mentioned above. The difference in the high voltage value which gives the same gas gain is about 200V. No appreciable difference was observed for the results with the

wire pattern No.1 and No.2, and with and without the magnetic field.

## 5. Position Measurement and Spatial Resolution

For the position measurement, the chamber was operated at the anode voltage of 2.3kV for the anode layers #1 and #4 - #10 and 2.5kV for the anode layers #2 and #3.

In the following analysis, we used the drift time information only from the test chamber.

At first, we assumed the relation between the drift time t and the beam position x on the anode wire plane as follows;

$$t = a - bx - cx^2, \qquad (1)$$

where t is given in nsec and x is given in cm. As the LRS 4291B TDC is used in a common-stop mode, the parameter b is positive. Parameters a, b and c are determined in the following steps;

(1) a is the time pedestal and determined as the maximum of the TDC distribution. The typical example of the drift time distribution is shown in Fig. 8.

(2) Since we analyzed the electron tracks perpendicular to the anode wire plane, we used another constraint for the x-t relation as follows; Figure 9 shows correlation of drift times $(t_1, t_2)$, obtained from two staggered layers. When the particle pass through the middle of the drift space, drift times $t_1$ and $t_2$ are the same. From this, the drift time for the half-cell was obtained.

(3) After the above, only one parameter remains and which was determined in such a way that the sum of residuals for the linear fit to each track is minimum.

(4) In the magnetic field, the x-t relation is different in the left and right drift cells. Therefore we determined the parameters b and c for the left and right cells separately.

Results of the determined parameters are shown in Table 1. The x-t relations are shown in Fig. 10. Without the magnetic field, the x-t relations are rather linear and do not depend on the wire pattern. However in the magnetic field of 6 kG, slight difference was observed at the far end of the drift space. The distortion of the equi-drift-time contour is less for the wire pattern No.2 than that for the wire pattern No.1.

The x-t plots for special anode wire planes #5 and #6 and their spatial resolutions are obtained in the following way; the track position on the anode wire plane #5 and #6 are determined from the data on other 8 layers of anode wire planes. Figure 11 shows the x-t scatter plot for the layers #5 and #6 of the No.2 pattern under various conditions. Without the magnetic field, the drift time is quite linear to the particle position. When the magnetic field of 6 kG is applied, deviation from the linear relation becomes apparent. For comparison with the drift time simulation, the calculated results are also shown in Fig. 11. The agreement between the experimental data and the calculation is reasonably good.

The spatial resolution is defined as a quadrutic mean of the difference between the position determined with the layer #5 and #6 and that determined by use of other 8 layers. The spatial resolution depends on various parameters and their characteristics are summarized in the following.

(a) H. V. dependence

Fig. 12 shows the H. V. dependence of the spatial resolution. The spatial resolution becomes slightly better as the H. V. increases. No difference was observed between the pattern No.1 and No.2. The mean spatial resolution is 110-120$\mu$m.

(b) Rate dependence

Fig. 13 shows the rate dependence of the spatial resolution. The x-t relation does not change for the particle rate up to 2.5 x $10^5$ particles/sec/wire. However the spatial resolution becomes worse when the particle rate exceeds 3 x $10^4$ particles/sec/wire.

(c) Magnetic field dependence

Fig. 14 shows the spatial resolution as a function of the magnetic field. The resolution becomes slightly worse when the magnetic field is applied. No appreciable difference was observed for the wire pattern No.1 and No.2.

(d) Position dependence of the spatial resolution

Fig. 15 shows the position dependence of the spatial resolution for various cases. Without the magnetic field, no big difference was observed for the wire pattern No.1 and No.2. However, when the magnetic field of 6 kG was applied, the spatial resolution near the wire position is much worse for the wire pattern No.1 than for the wire pattern No.2. This is because the distortion of the equi-drift-time contour is bigger for the wire pattern No.1 than for the wire pattern No.2.

## 6. Summary

Among two wire patterns tested for the TOPAZ inner drift chamber, the hexagonal drift cell (No.2) resulted in a better x-t relation than the square drift cell (No.1). The simulation of the x-t relation well reproduced the experimental data. The spatial resolution obtained for both cases is 110 $\mu$m with the gas mixture of Ar(50)/$C_2H_6$(50).

Thus we chose the hexagonal cell for the TOPAZ IDC. Further improvements on the tracking software is now under study.

The authers express their sincere thanks to the INS synchrotron staff for their help in various stages of the experiment. The numerical calculation and data analysis were done by use of FACOM M380R at the INS Computer Facilities.

## References

1) TRISTAN Proposal, TRISTAN-EXP-002, study of $e^+e^-$ Annihilation Phenomena by a Detector with Particle Identification, by TOPAZ Collaboration (January 1983).

2) K. Shiino et. al., INS-TH-159 and INS-TOPAZ. 84/4, Test of the Delay Line for Z-readout of the TOPAZ Inner Drift Chamber (April,1984).

3) K. Fujii et. al., DPNU-84-02, Performance of Limited Streamer Drift Tubes (Jan. 1984).

Figure Captions

Fig. 1 TOPAZ Inner Drift Chamber.

Fig. 2 End-plate configuration.

Fig. 3 Wire patterns of the test drift chamber.

Fig. 4 Equi-drift-time maps for two wire patterns. (a) No. 1, the square drift cell and (b) No.2, the hexagonal drift cell.

Fig. 5 Experimental setup.

Fig. 6 Collected charge distributions for $^{55}Fe$ X-rays and 500 MeV/c electrons. (a) H.V. = 2.1 kV, (b) H.V. = 2.2kV, (c) H.V. = 2.3 kV. (d) H.V.= 2.4 kV. The position of the peak is adjusted to be the same on the display.

Fig. 7 Efficiency curves for the minimum-ionizing particles in $Ar(50\%)/C_2H_6(50\%)$. (a) the results without magnetic field and (b) the results with magnetic field of 6 kG.

Fig. 8 Typical drift-time distribution in the No.2 chamber. (a) B = 0 kG and (b) B = 6 kG. The particle distribution over the drift cell is uniform.

Fig. 9 Scatter plot of drift times, $t_1$ and $t_2$ on two staggered anode wires. (a) B = 0 kG and (b) B = 6 kG.

Fig.10 The x-t relations obtained from the fitting. (a) and (b) : H.V. dependence. (c) and (d) : magnetic field dependence.

Fig.11 The x-t scatter plots for the anode wires on the 5-th and 6-th layers in the No.2 chamber. Solid lines show the results of the simulation. (a) B = 0 kG and (b) B = 6 kG.

Fig.12 High-voltage dependence of the spatial resolution.

Fig.13 Rate dependence of the spatial resolution.

Fig.14 Magnetic-field dependence of the spatial resolution.

Fig.15 Position dependence of the spatial resolution.
(a) B = 0 kG and (b) B = 6 kG.

Table 1. Results of the x-t relation fitted with the function $x = a - bt - ct^2$.

(a) H.V. dependence

| | H.V.(kV) | a | b | c |
|---|---|---|---|---|
| No.1 | 2.25 | 378 | 179.6 | 56.9 |
| | 2.30 | 379 | 190.8 | 30.7 |
| | 2.40 | 380 | 196.4 | 12.0 |
| | 2.50 | 381 | 193.2 | 22.7 |
| | H.V.(kV) | a | b | c |
| No.2 | 2.20 | 377 | 174.8 | 61.8 |
| | 2.25 | 378 | 178.8 | 48.4 |
| | 2.30 | 379 | 186.8 | 32.9 |
| | 2.35 | 380 | 188.4 | 27.6 |
| | 2.40 | 381 | 192.4 | 25.3 |

(b) Rate dependence

| | Rate(kHz) | a | b | c |
|---|---|---|---|---|
| No.1 | 1.8 | 379 | 192.4 | 25.3 |
| | 6.0 | 379 | 194.0 | 20.0 |
| | 16 | 379 | 192.4 | 25.3 |
| | 38 | 378 | 190.8 | 30.7 |
| | 144 | 377 | 182.0 | 60.0 |
| | 264 | 376 | 187.6 | 41.3 |
| | Rate(kHz) | a | b | c |
| No.2 | 4.1 | 379 | 170.0 | 66.7 |
| | 32 | 378 | 167.6 | 74.7 |
| | 100 | 377 | 171.6 | 72.4 |

(c) Magnetic field dependence

| | B(kG) | a | $b_R$ | $c_R$ | $b_L$ | $c_L$ |
|---|---|---|---|---|---|---|
| No.1 | 0 | 379 | 190.8 | 30.7 | 190.8 | 30.7 |
| | 2 | 379 | 182.0 | 37.8 | 165.2 | 71.6 |
| | 4 | 379 | 137.2 | 187.1 | 170.0 | 66.7 |
| | 6 | 379 | 149.6 | 179.1 | 195.6 | 14.6 |
| | B(kG) | a | $b_R$ | $c_R$ | $b_L$ | $c_L$ |
| No.2 | 0 | 379 | 186.8 | 32.9 | 186.8 | 32.9 |
| | 2.6 | 379 | 194.4 | 7.6 | 182.8 | 35.1 |
| | 4.3 | 379 | 187.2 | 42.7 | 178.8 | 48.4 |
| | 6 | 379 | 169.6 | 112.4 | 179.6 | 45.8 |

# TOPAZ ; INNER DRIFT CHAMBER

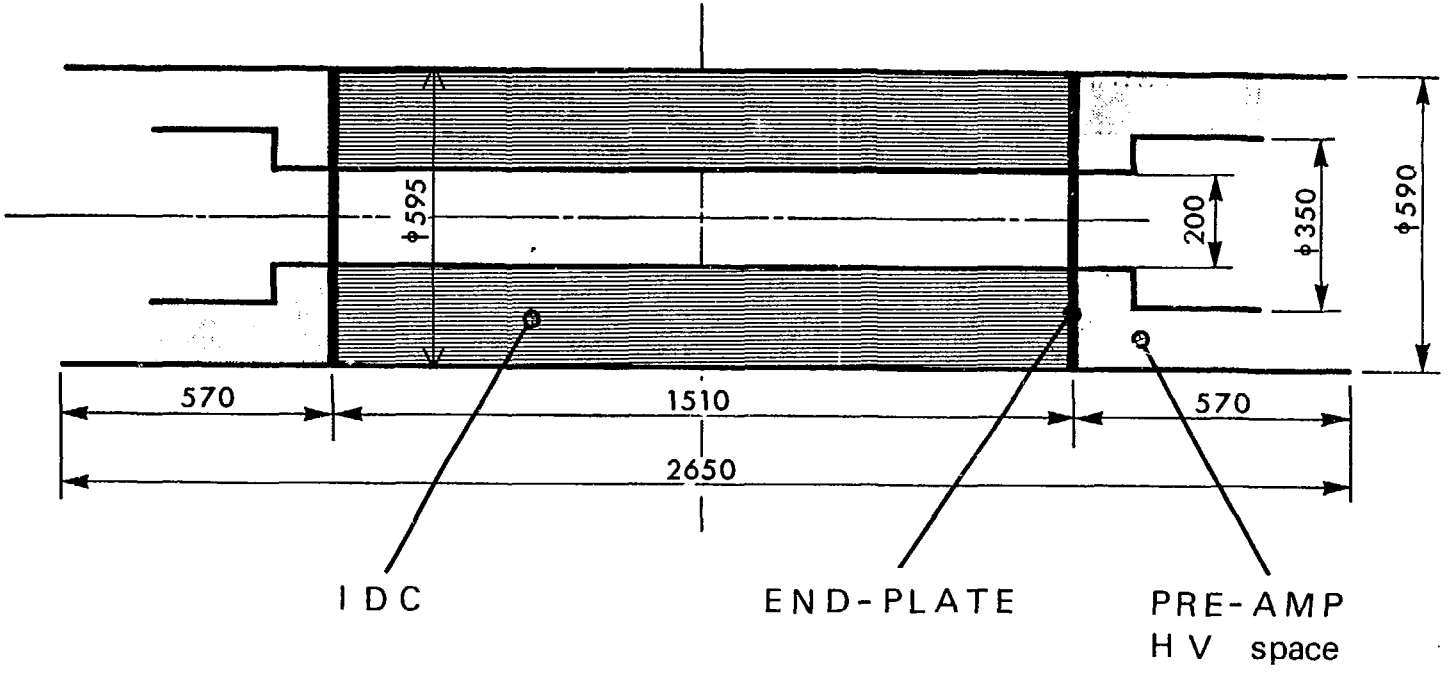


Fig . 1

TRISTAN (TOPAZ) IDC END PLATE

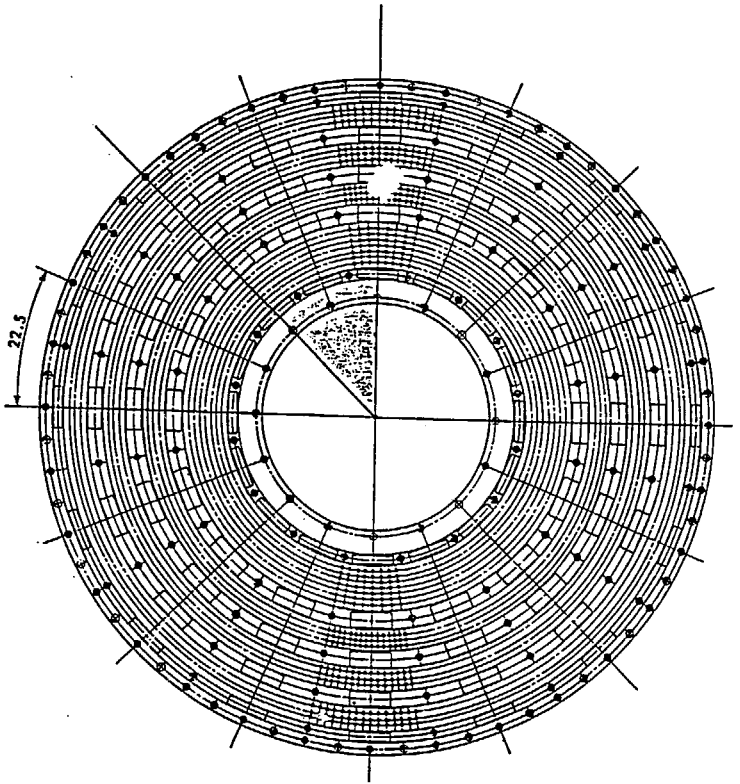


Inner Drift Chamber

(Part)

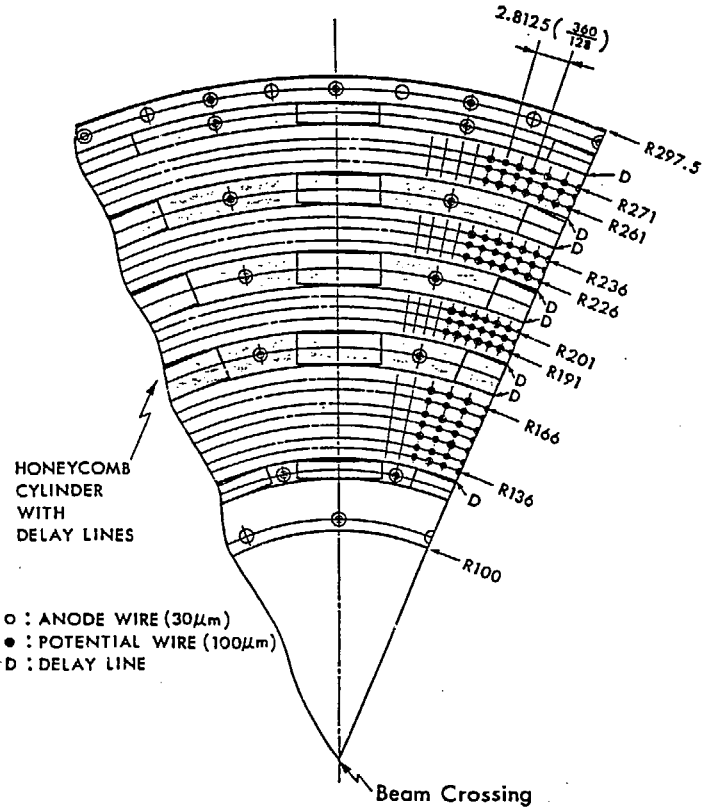


Fig . 2

(a) No.1 Square Cell

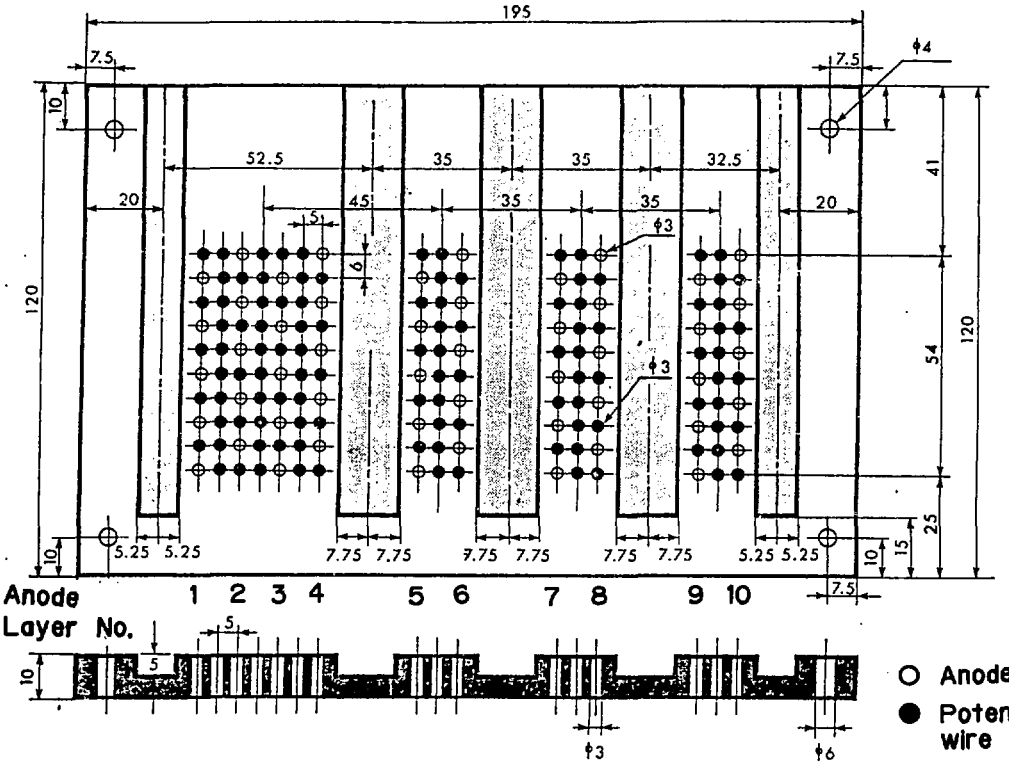


(b) No.2 Hexagonal Cell

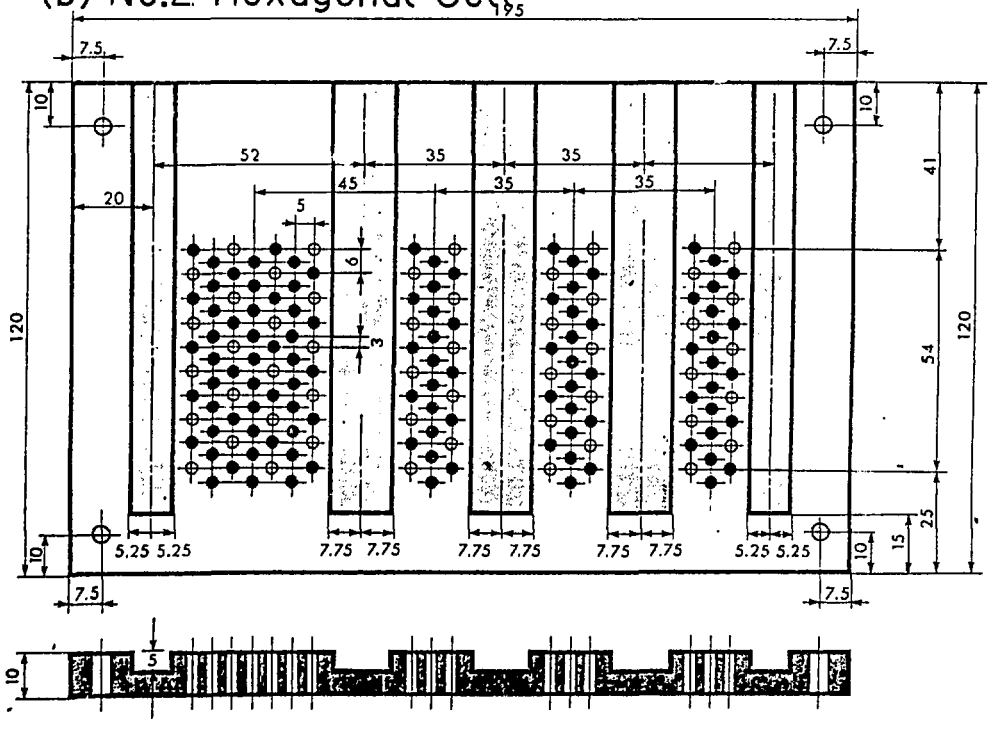


Fig . 3

(a) No 1

(A. B. C. D) = (-20. 0. -6. 0. 20. 0. 16. 0)

B = 0 Gauss

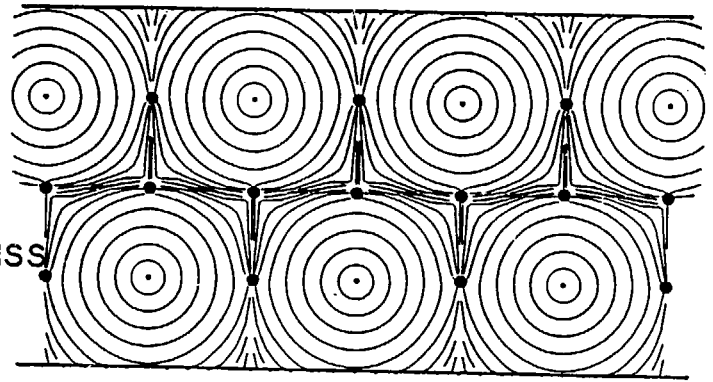

EQUI-DRIFT TIME MAP: TIME STEP= 20. ONSEC
MAG. FIELD: (BX. BY. BZ) = ( 0. 00. 0. 00. 0. 00)

(A. B. C. D) = (-20. 0. -6. 0. 20. 0. 16. 0)

B = 6K Gauss

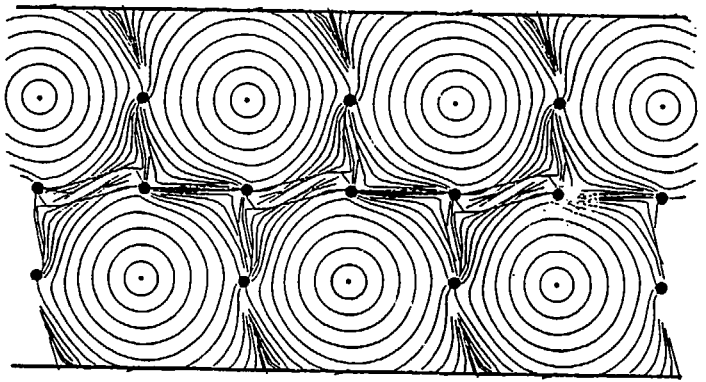

EQUI-DRIFT TIME MAP: TIME STEP= 20. ONSEC
MAG. FIELD: (BX. BY. BZ) = ( 0. 00. 0. 00. 0. 60)

(b) No 2

(A, B. C. D) = (-20. 0. -6. 0. 20. 0. 16. 0)

B = 0 Gauss

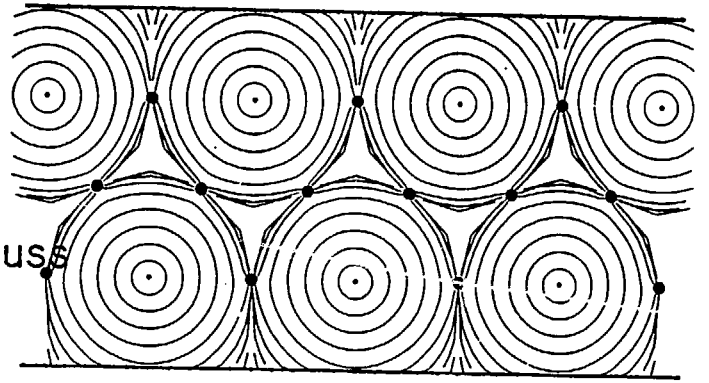

EQUI-DRIFT TIME MAP: TIME STEP= 20. ONSEC
MAG. FIELD: (BX. BY. BZ) = ( 0. 00. 0. 00. 0. 00)

(A. B. C. D) = (-20. 0. -6. 0. 20. 0. 16. 0)

B = 6K Gauss

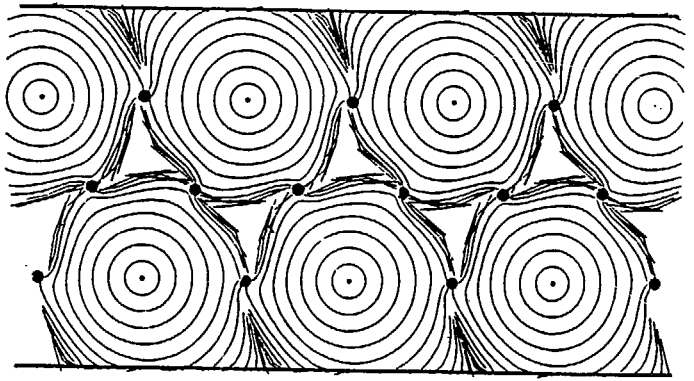

EQUI-DRIFT TIME MAP: TIME STEP= 20. ONSEC
MAG. FIELD: (BX. BY. BZ) = ( 0. 00. 0. 00. 0. 60)



Fig . 4

# SET UP OF DC TEST

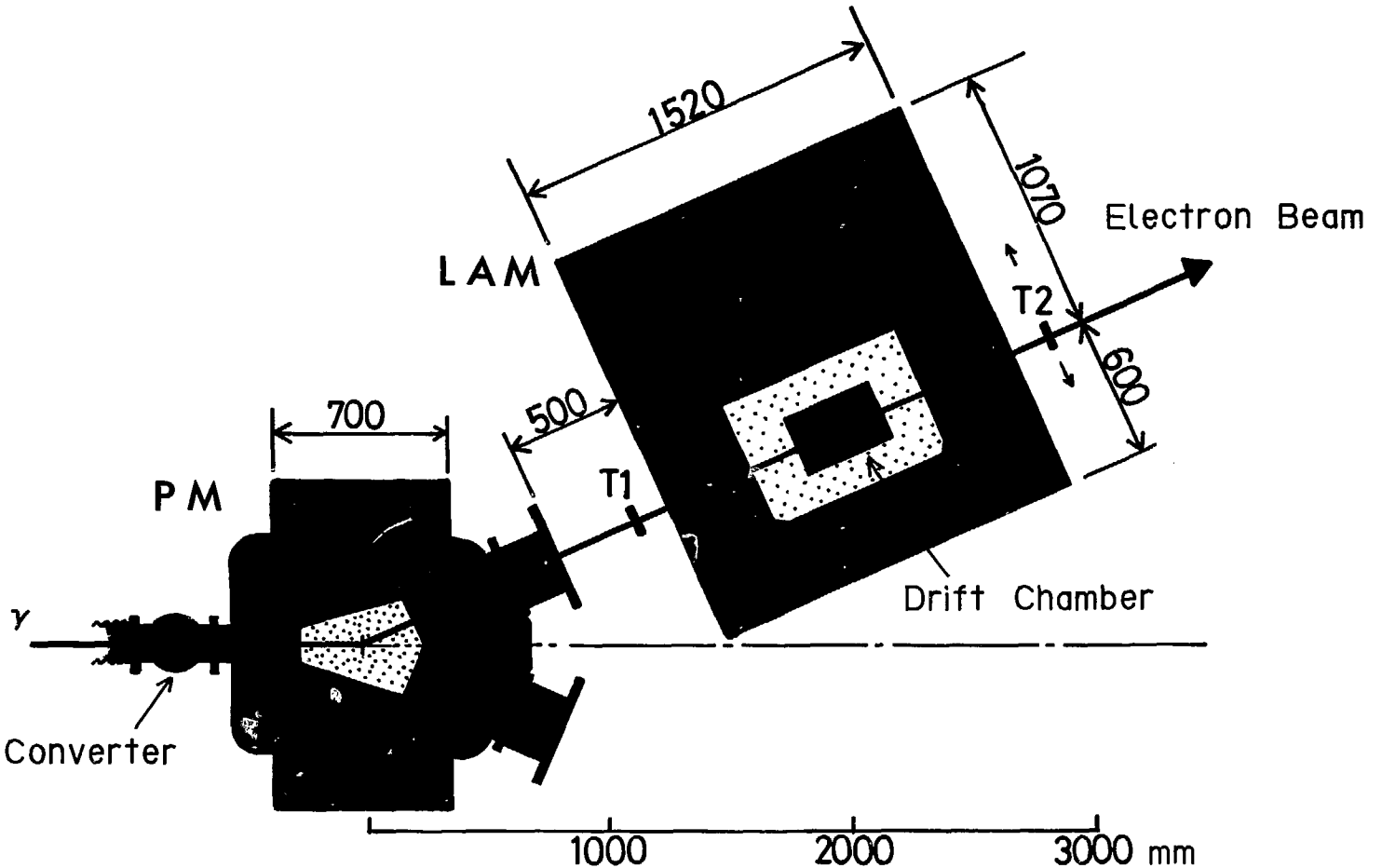


Fig . 5

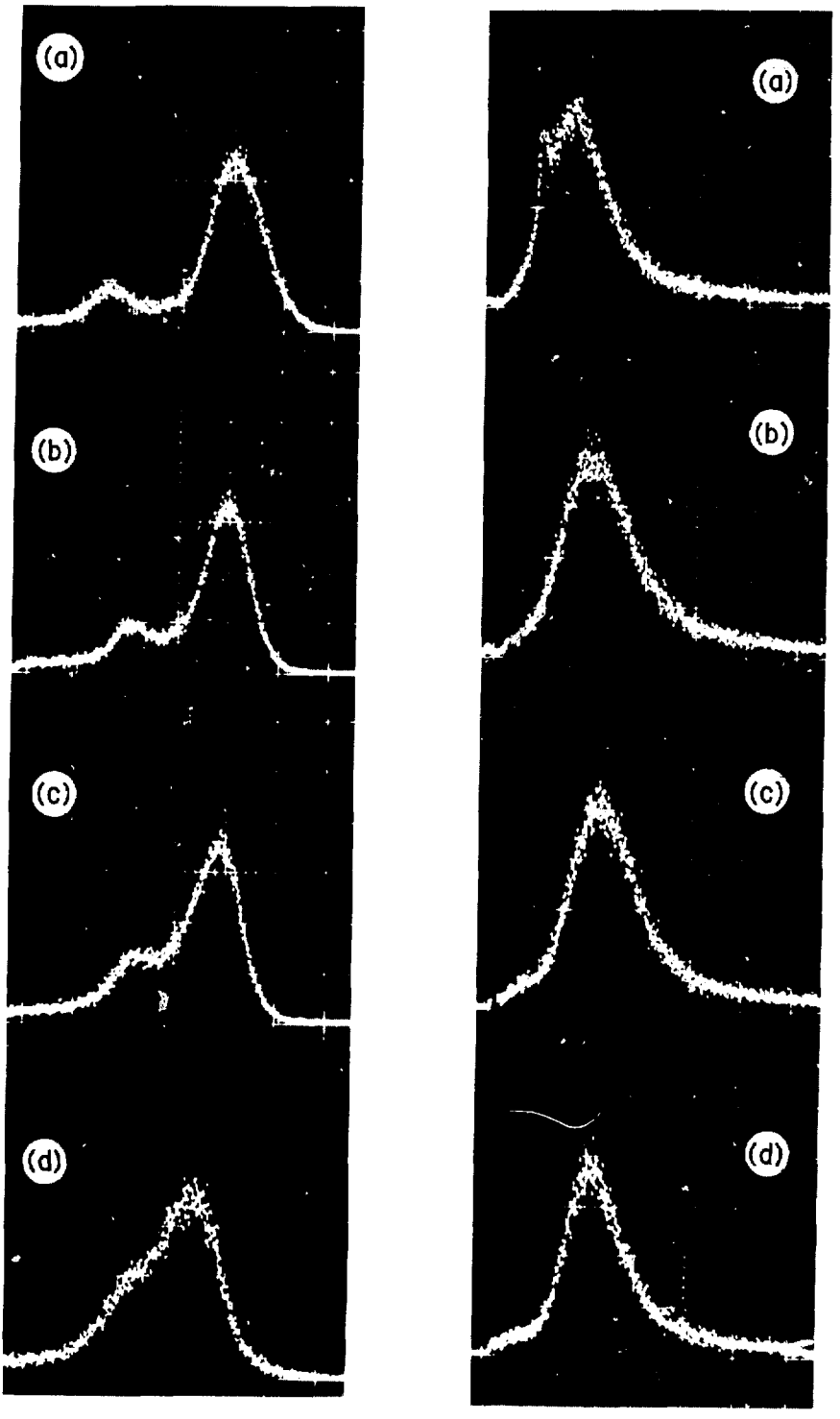




Fig. 6

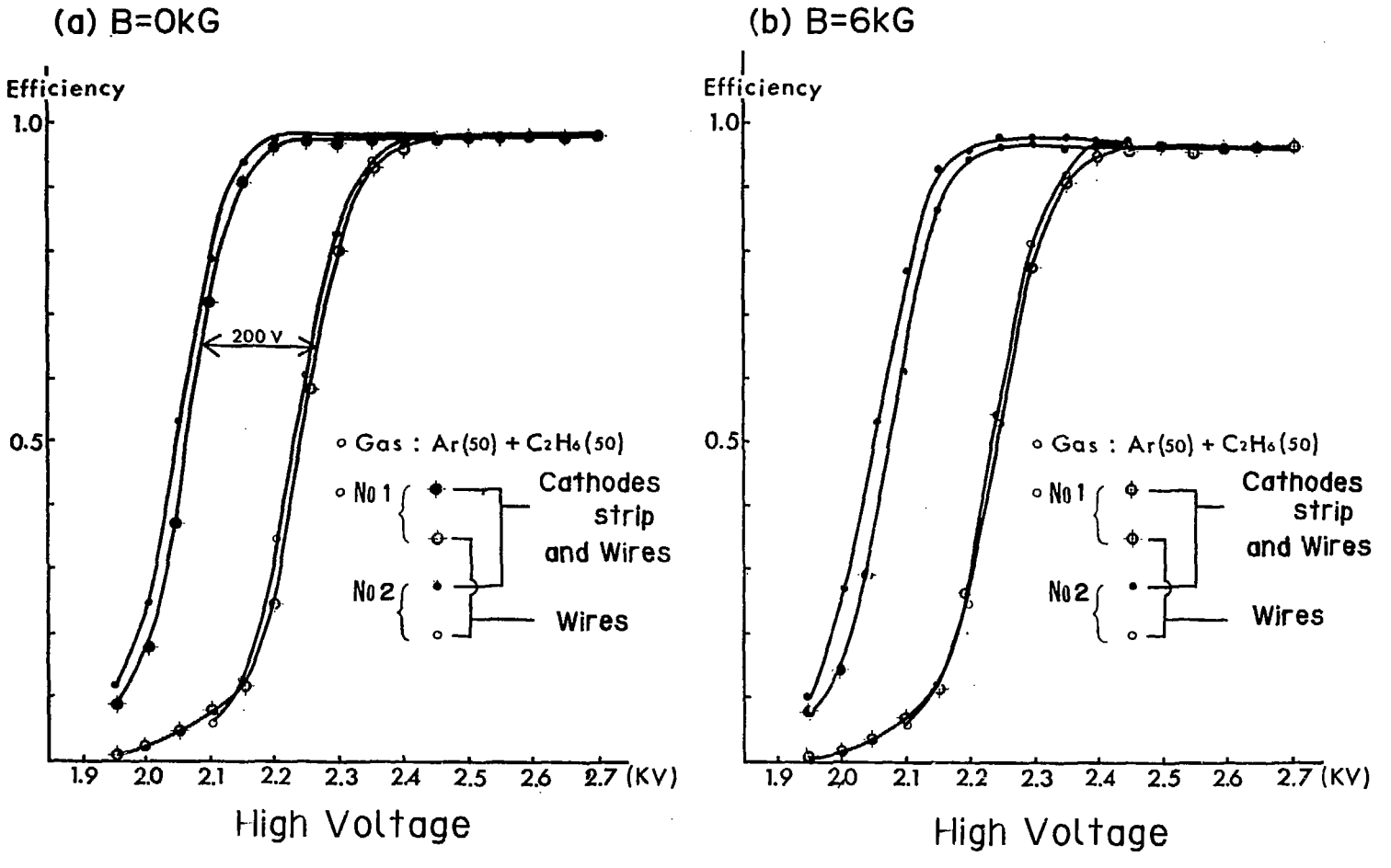
(a) B=0kG
Efficiency
1.0
0.5
200 V
∘ Gas : Ar(50) + C2H6(50)
∘ No 1
No 2
Cathodes strip and Wires
Wires
1.9 2.0 2.1 2.2 2.3 2.4 2.5 2.6 2.7 (KV)
High Voltage
(b) B=6kG
Efficiency
1.0
0.5
∘ Gas : Ar(50) + C2H6(50)
∘ No 1
No 2
Cathodes strip and Wires
Wires
1.9 2.0 2.1 2.2 2.3 2.4 2.5 2.6 2.7 (KV)
High Voltage

Fig . 7

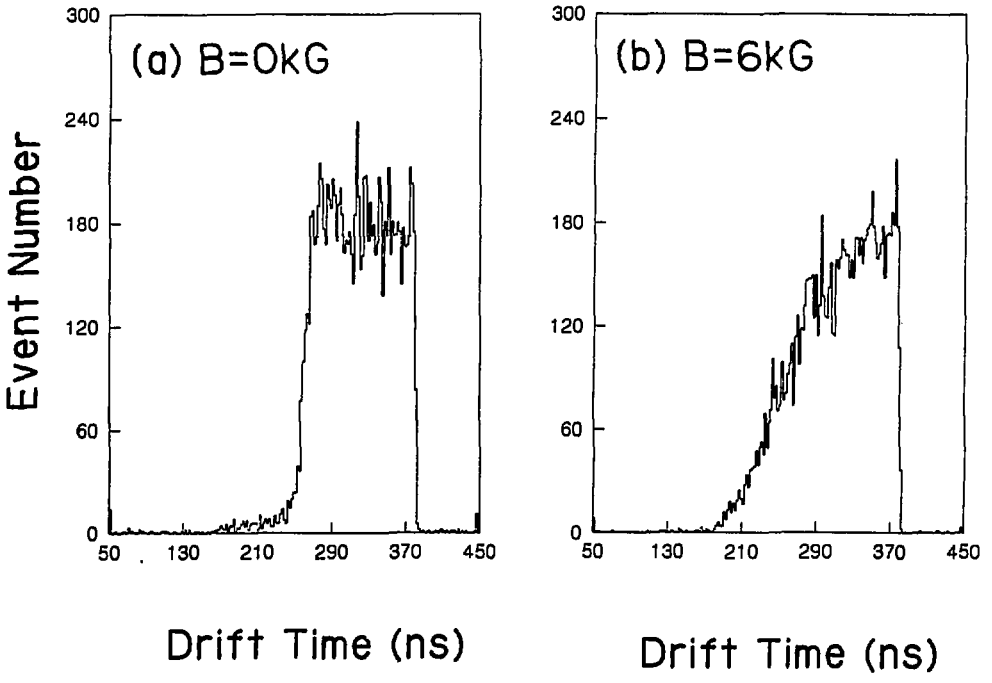
(a) B=0kG
(b) B=6kG
Event Number
300
240
180
120
60
0
50
130
210
290
370
450
Drift Time (ns)
Drift Time (ns)

Fig. 8

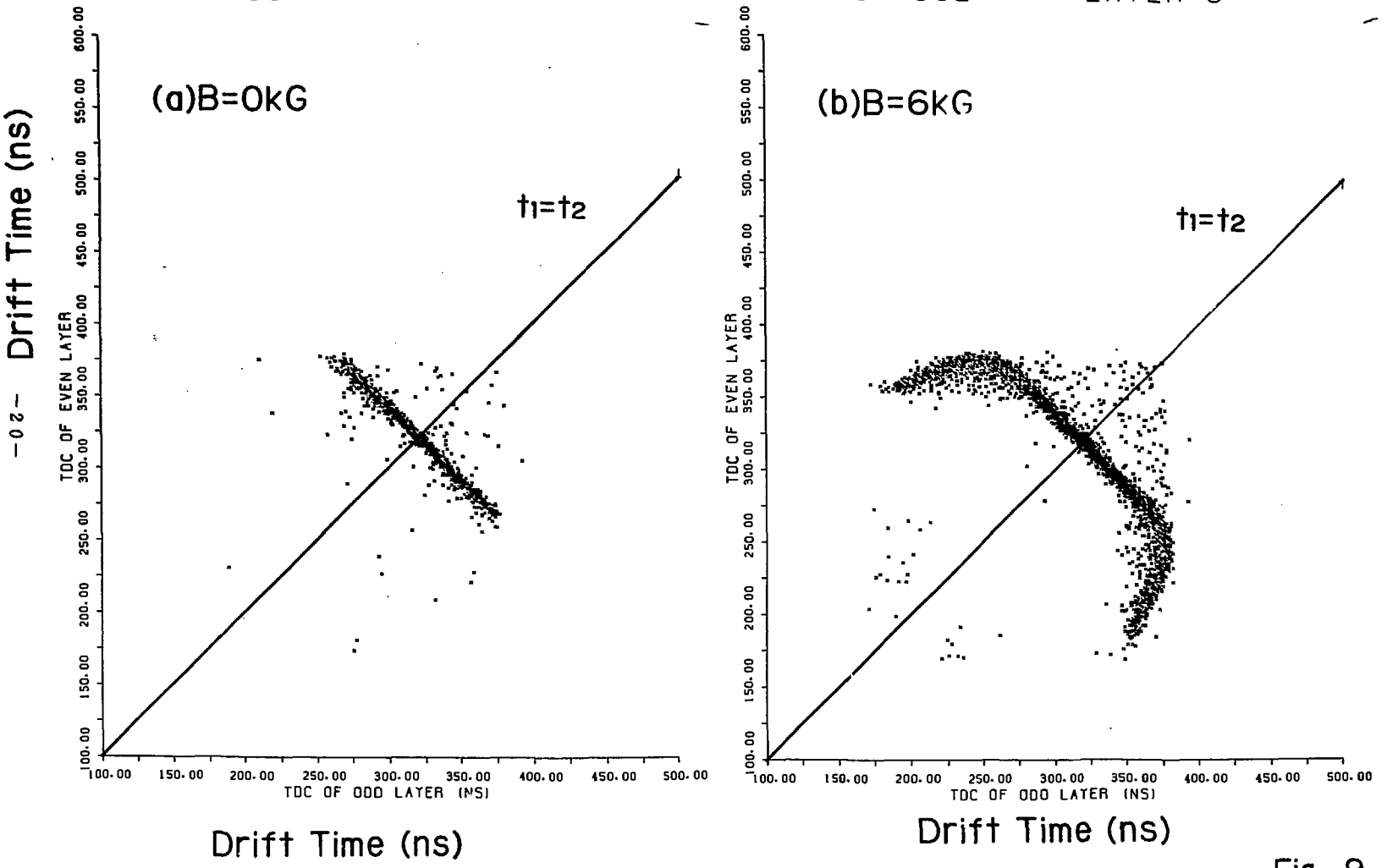
RUN 312 LAYER 3
(a)B=0kG
t1=t2
TDC OF EVEN LAYER
TDC OF ODD LAYER (NS)
Drift Time (ns)
Drift Time (ns)
RUN 332 LAYER 3
(b)B=6kG
t1=t2
TDC OF EVEN LAYER
TDC OF ODD LAYER (NS)
Drift Time (ns)

Fig. 9

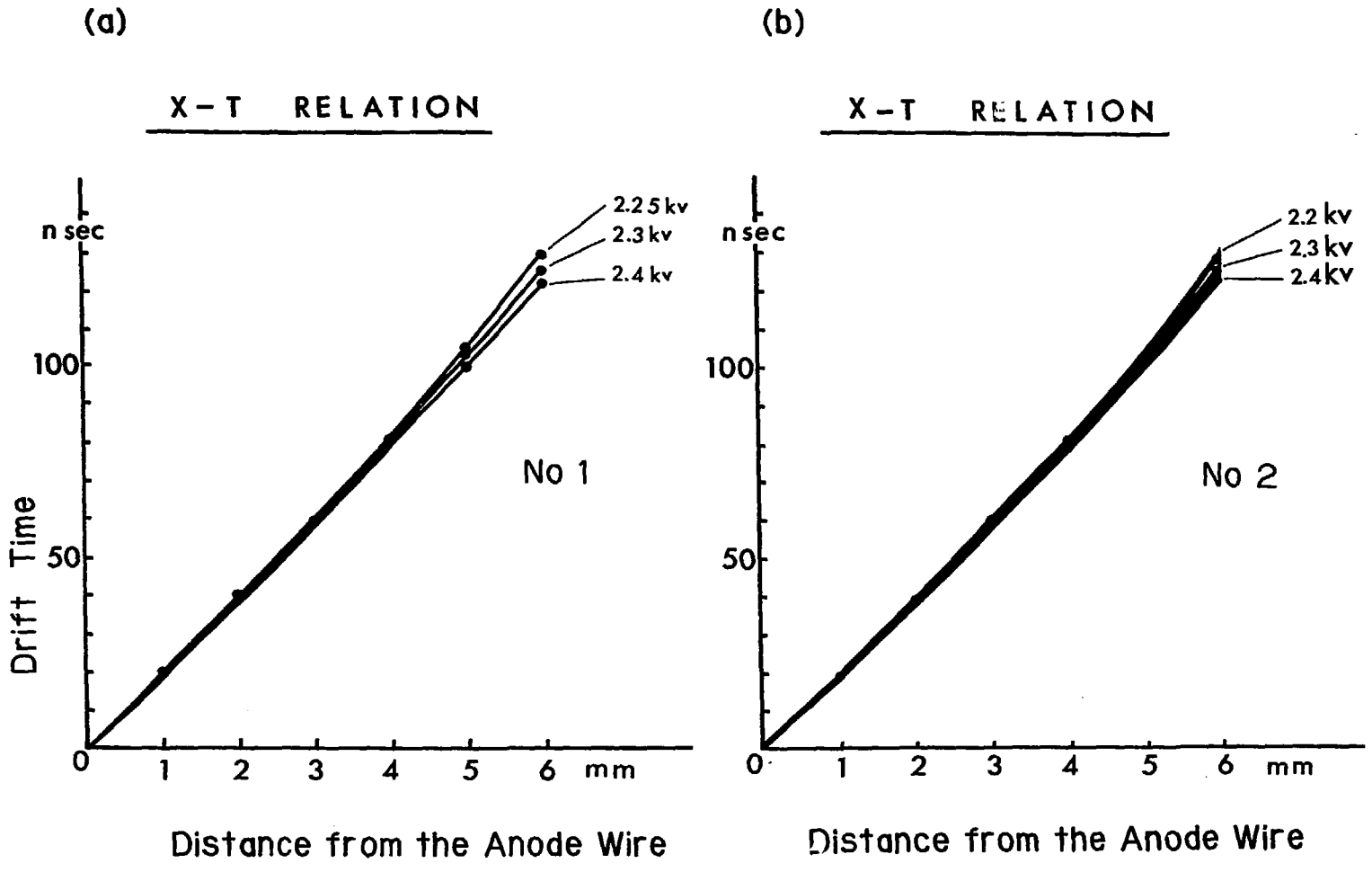
(a)
X-T RELATION
n sec
100
50
0
Drift Time
2.25 kv
2.3 kv
2.4 kv
No 1
1
2
3
4
5
6 mm
Distance from the Anode Wire
(b)
X-T RELATION
n sec
100
50
0
2.2 kv
2.3 kv
2.4 kv
No 2
1
2
3
4
5
6 mm
Distance from the Anode Wire

Fig . 10

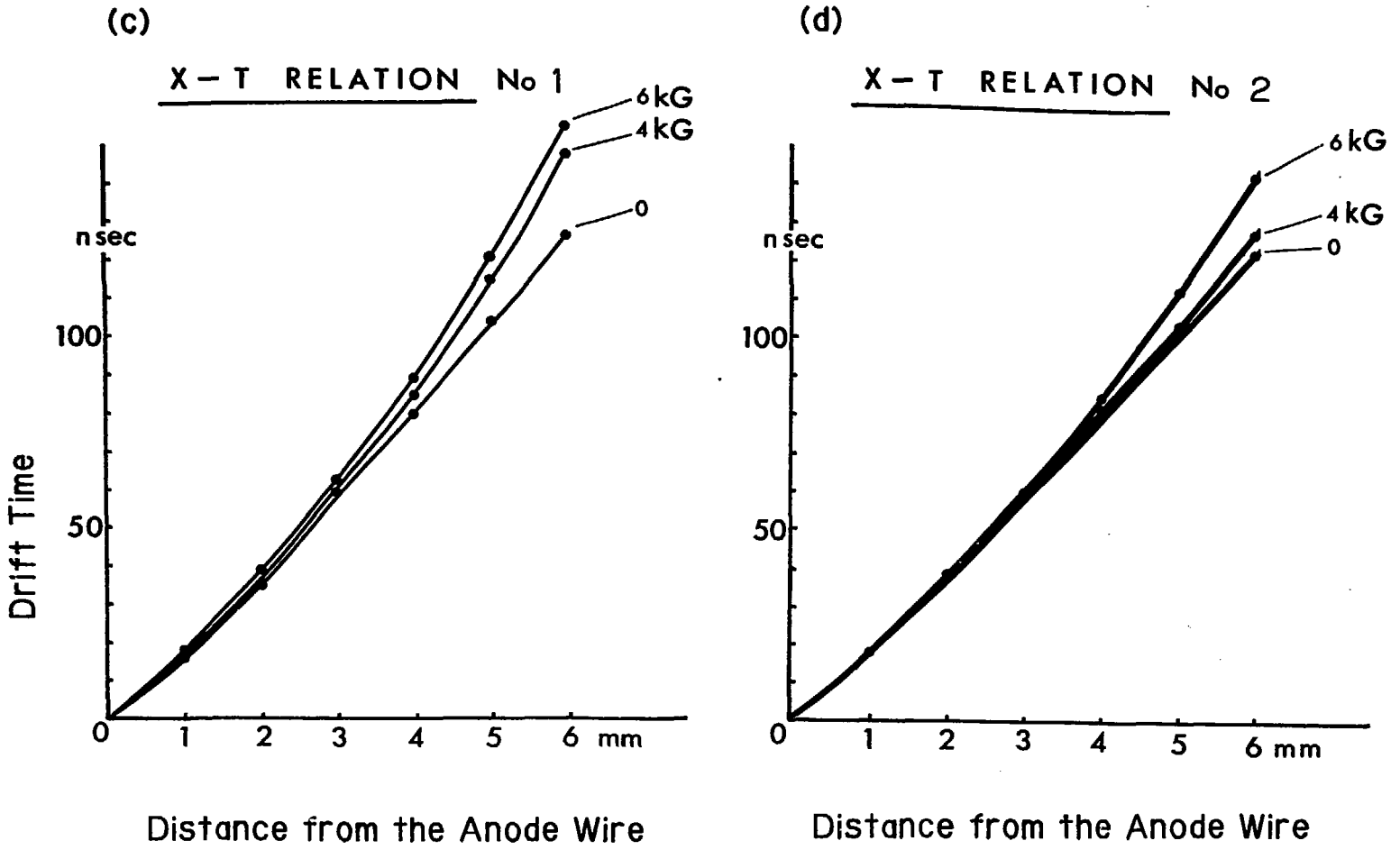
(c)
X – T RELATION No 1
6 kG
4 kG
0
n sec
100
50
0
1
2
3
4
5
6 mm
Drift Time
Distance from the Anode Wire
(d)
X – T RELATION No 2
6 kG
4 kG
0
n sec
100
50
0
1
2
3
4
5
6 mm
Distance from the Anode Wire

Fig . 10

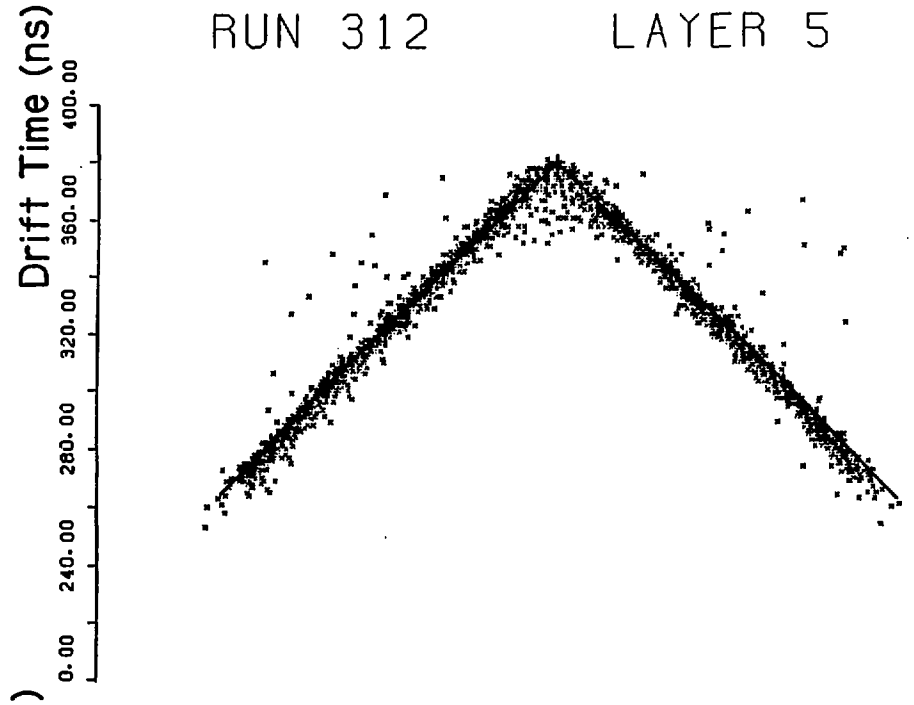
RUN 312
LAYER 5
Drift Time (ns)
0.00
240.00
280.00
320.00
360.00
400.00

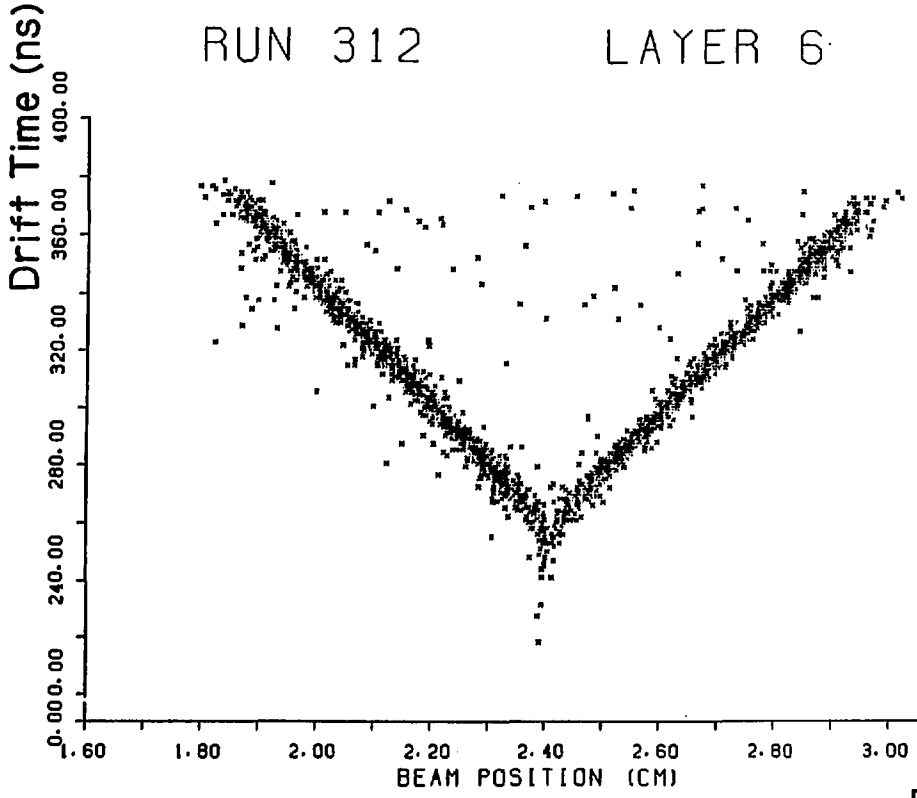
RUN 312
LAYER 6
Drift Time (ns)
0.000.00
240.00
280.00
320.00
360.00
400.00
1.60
1.80
2.00
2.20
2.40
2.60
2.80
3.00
3.20
BEAM POSITION (CM)

Fig . 11(a)

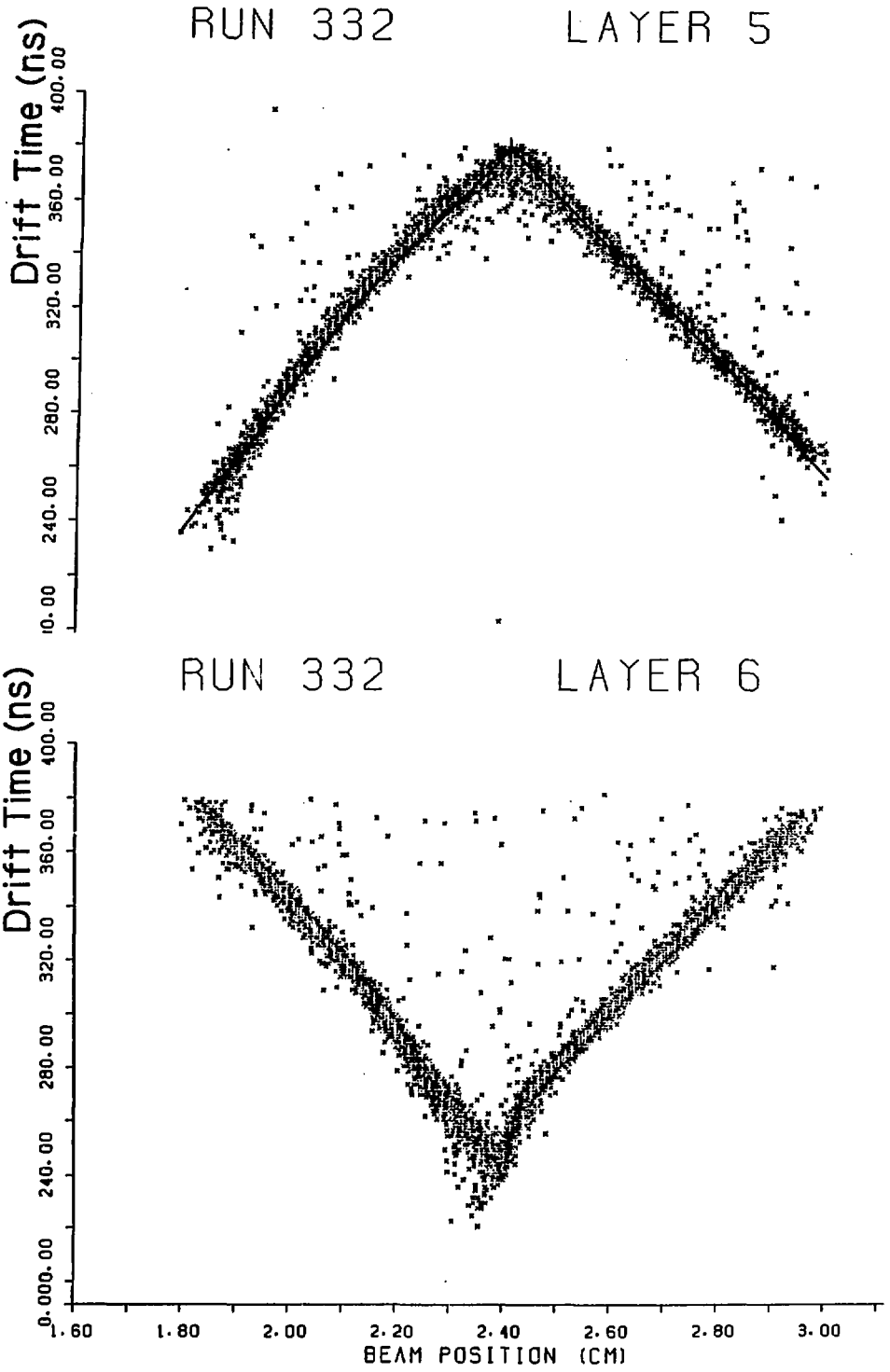
RUN 332
LAYER 5
Drift Time (ns)
400.00
360.00
320.00
280.00
240.00
10.00
RUN 332
LAYER 6
Drift Time (ns)
400.00
360.00
320.00
280.00
240.00
0.000.00
1.60
1.80
2.00
2.20
2.40
2.60
2.80
3.00
BEAM POSITION (CM)



Fig . 11(b)

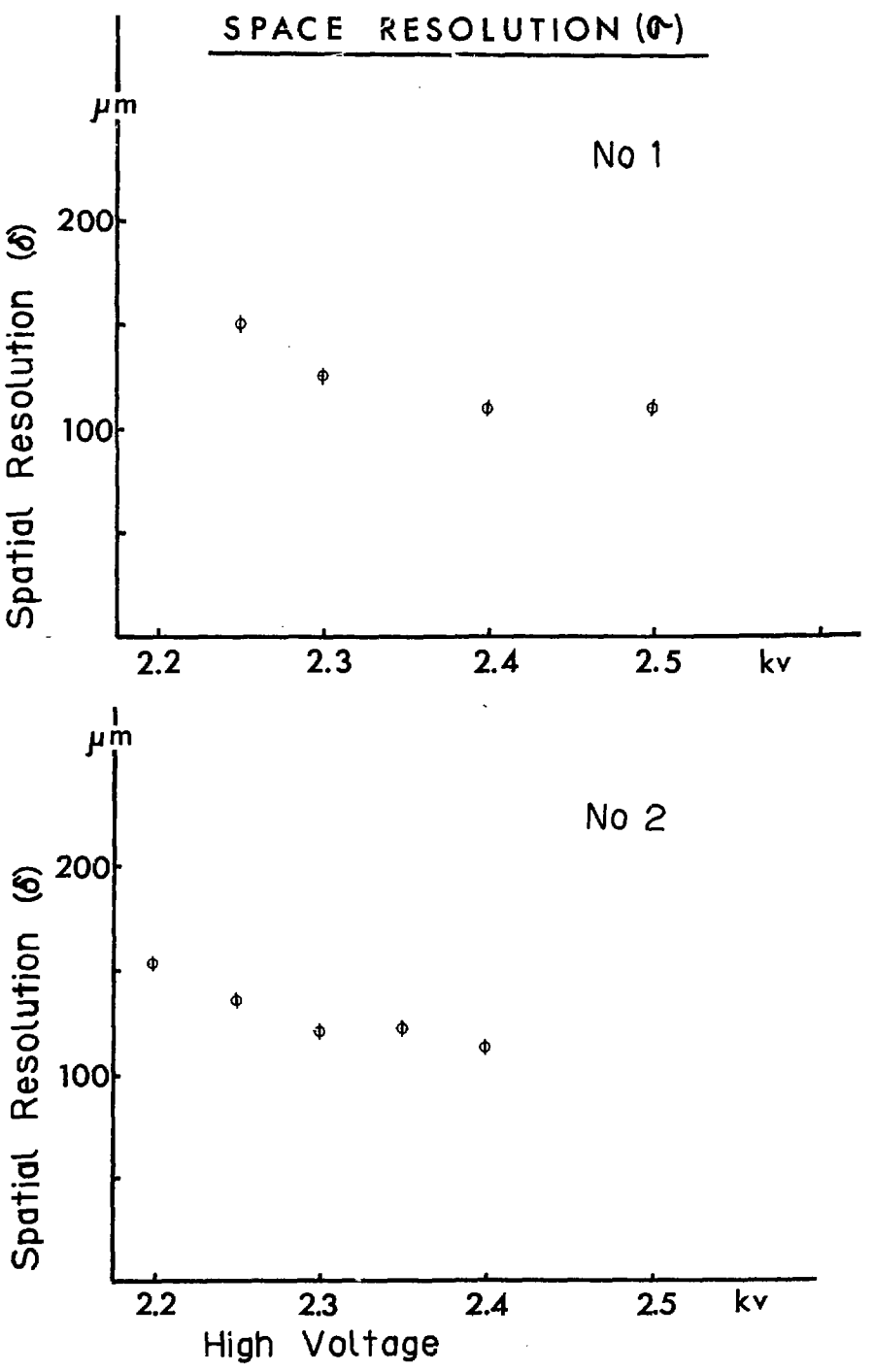
HV DEPENDENCE
SPACE RESOLUTION (σ)
μm
No 1
200
100
Spatial Resolution (σ)
2.2
2.3
2.4
2.5
kv
μm
No 2
200
100
Spatial Resolution (σ)
2.2
2.3
2.4
2.5
kv
High Voltage

Fig . 12

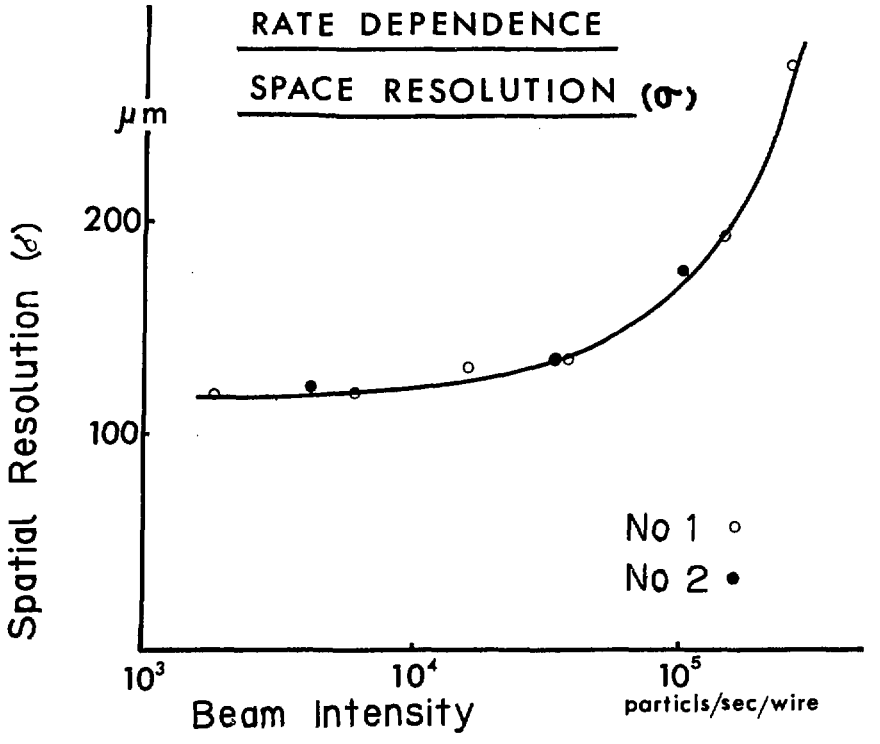
RATE DEPENDENCE
SPACE RESOLUTION (σ)
μm
200
100
Spatial Resolution (σ)
No 1 ○
No 2 ●
10³
10⁴
10⁵
Beam Intensity
particls/sec/wire

Fig . 13

## MAGNETIC FIELD DEPENDENCE

### SPACE RESOLUTION (σ)

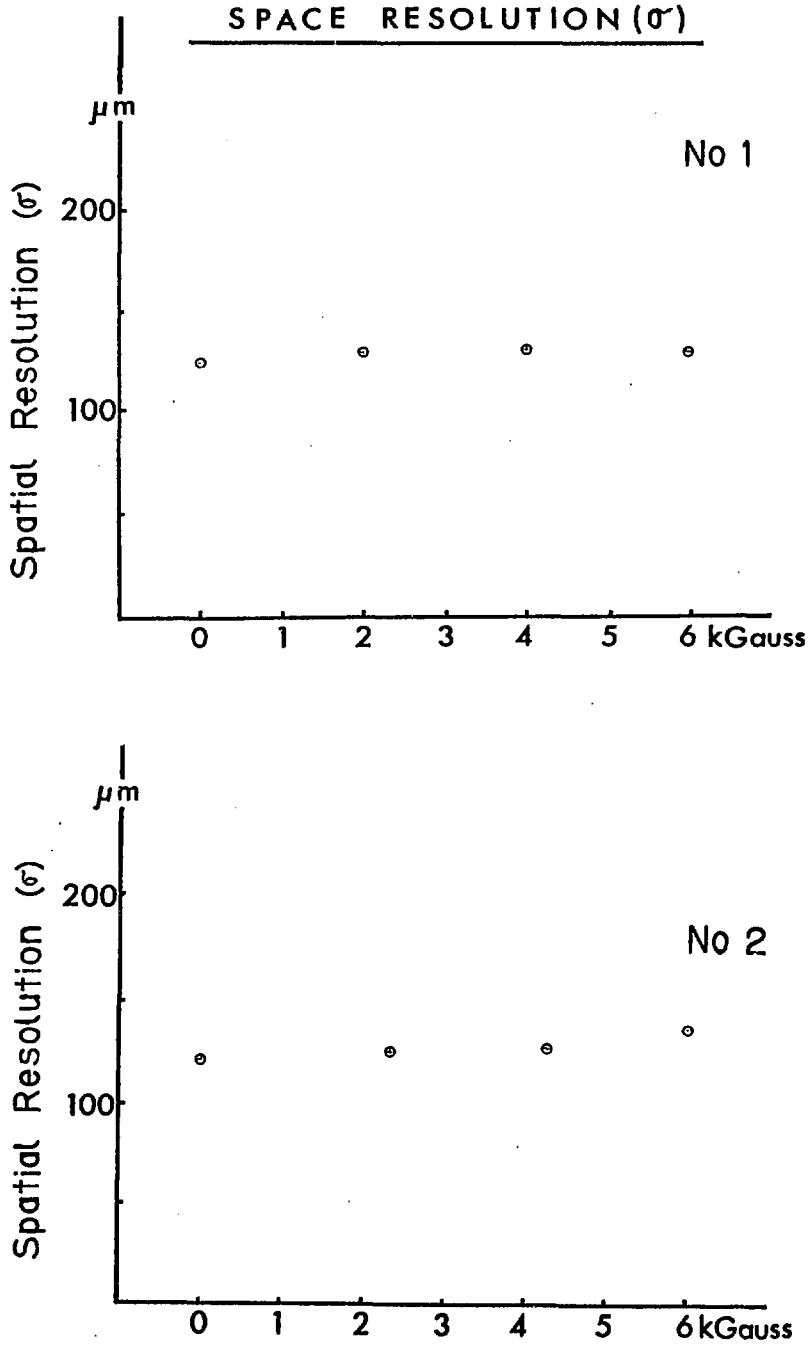


Fig. 14

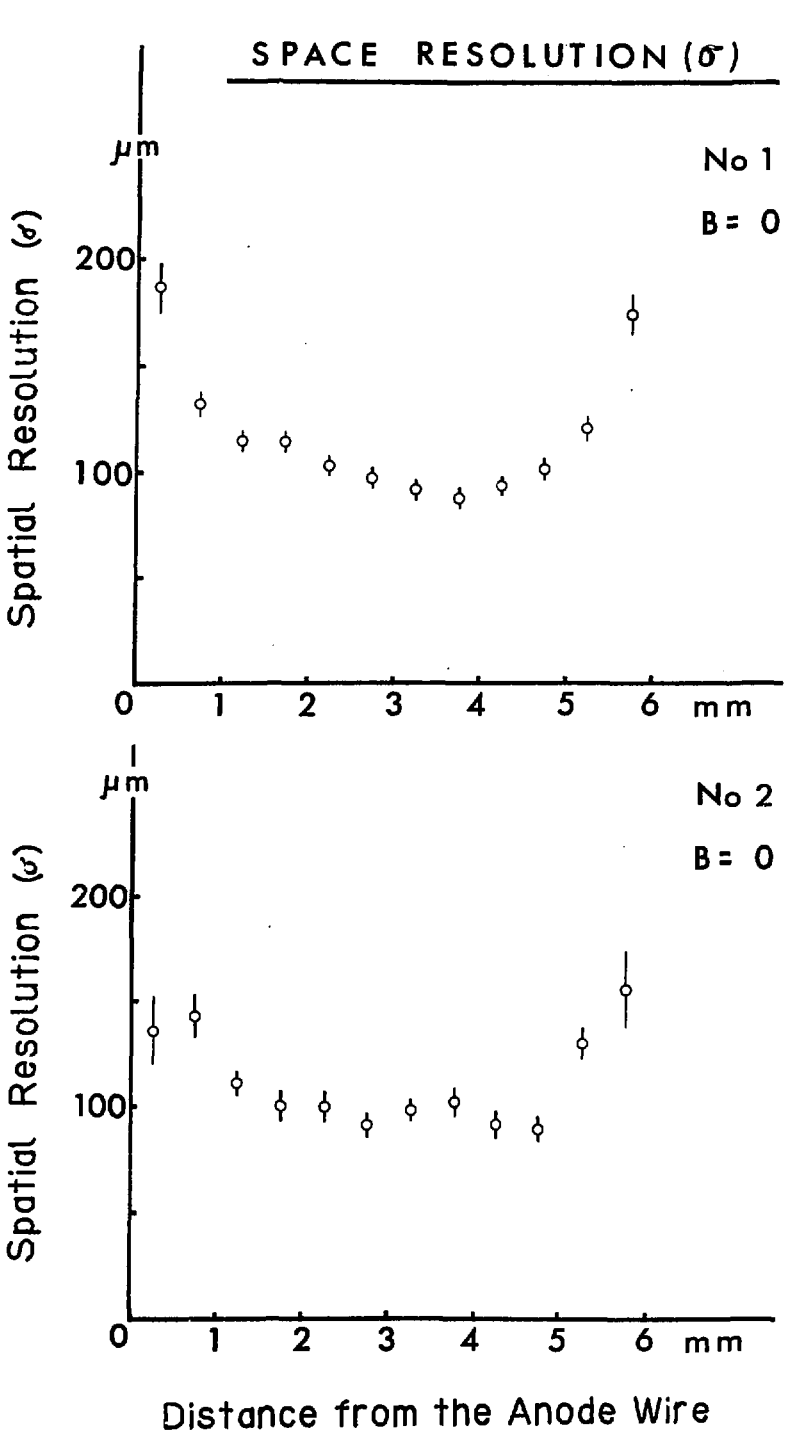
POSITION DEPENDENCE
SPACE RESOLUTION (σ)
μm
No 1
B = 0
200
100
0
1
2
3
4
5
6
mm
Spatial Resolution (σ)
μm
No 2
B = 0
200
100
0
1
2
3
4
5
6
mm
Spatial Resolution (σ)
Distance from the Anode Wire

Fig . 15 (a)

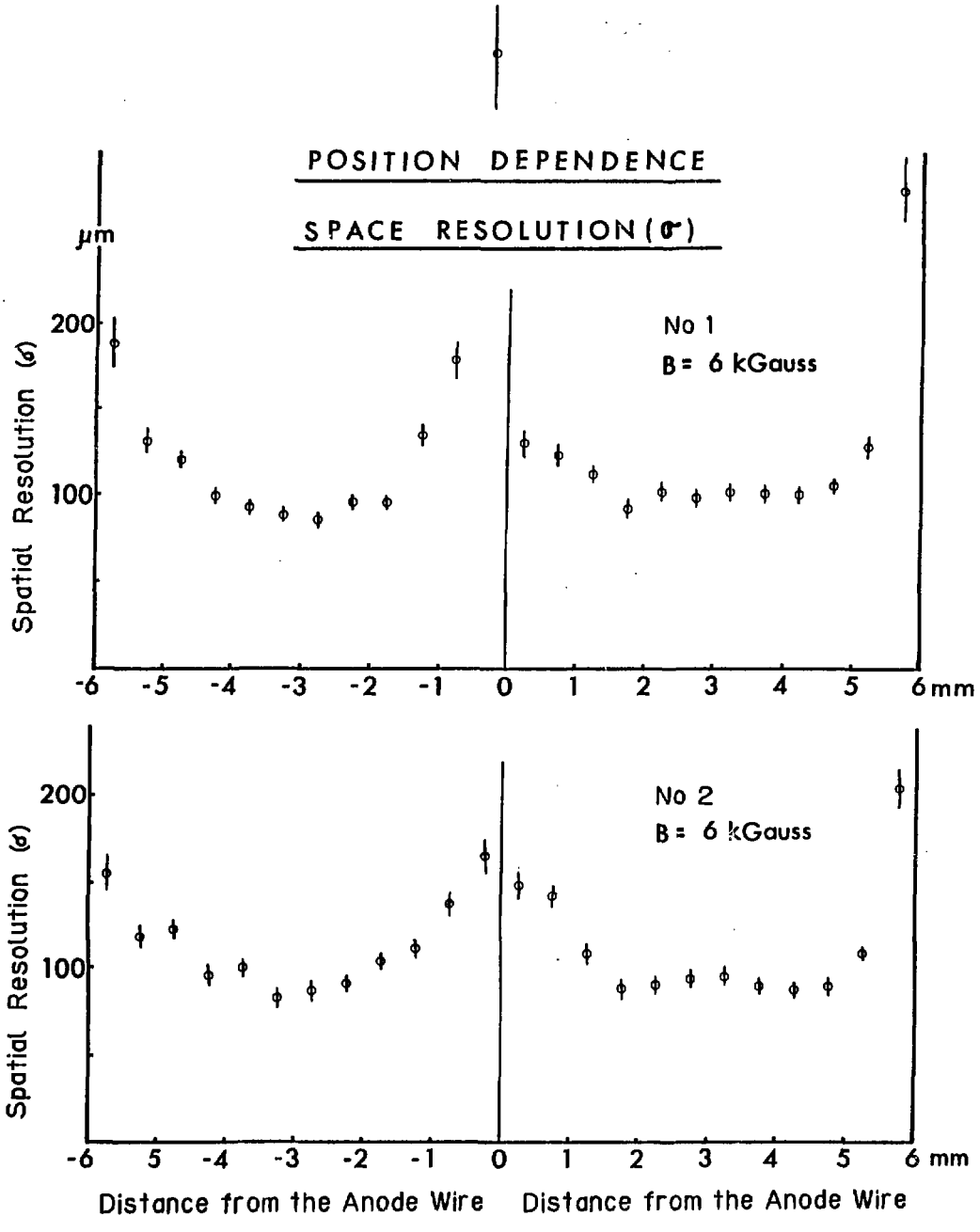
POSITION DEPENDENCE
SPACE RESOLUTION (σ)
μm
Spatial Resolution (σ)
200
100
No 1
B = 6 kGauss
-6 -5 -4 -3 -2 -1 0 1 2 3 4 5 6mm
Spatial Resolution (σ)
200
100
No 2
B = 6 kGauss
-6 5 -4 -3 -2 -1 0 1 2 3 4 5 6 mm
Distance from the Anode Wire
Distance from the Anode Wire

Fig . 15(b)